Public Health England

Protecting and improving the nation's health

Technical evaluation of Philips MicroDose SI digital mammography system

NHS Breast Screening Programme Equipment Report 1310

February 2016

Public Health England leads the NHS Screening Programmes

About Public Health England Screening

Screening identifies apparently healthy people who may be at increased risk of a disease or condition, enabling earlier treatment or better informed decisions. National population screening programmes are implemented in the NHS on the advice of the UK National Screening Committee (UK NSC), which makes independent, evidence-based recommendations to ministers in the 4 UK countries. The Screening Quality Assurance Service (SQAS) ensures programmes are safe and effective by checking that national standards are met.

Public Health England (PHE) leads the NHS Screening Programmes and hosts the UK NSC secretariat. PHE is an executive agency of the Department of Health and exists to protect and improve the nation's health and wellbeing, and reduce health inequalities.

PHE Screening
Floor 2, Zone B
Skipton House
80 London Road
London SE1 6LH
www.gov.uk/topic/population-screening-programmes
Twitter: @PHE_Screening Blog: phescreening.blog.gov.uk

Prepared by: KC Young, CJ Strudley
For queries relating to this document, please contact:
PHE.screeninghelpdesk@nhs.net

Published March 2016
PHE publications gateway number: 2015714

Acknowledgements

The authors are grateful to the staff at the Breast Unit at Addenbrooke's Hospital, Cambridge, for their cooperation in the evaluation of the system at their site.

Document Information	
Title	Technical evaluation of Philips MicroDose SI digital mammography system
Policy/document type	Equipment Report 1310
Electronic publication date	February 2016
Version	1
Superseded publications	None
Review date	None
Author/s	KC Young CJ Strudley
Owner	NHS Breast Screening Programme
Document objective (clinical/healthcare/social questions covered)	To provide an evaluation of this equipment's suitability for use within the NHSBSP
Population affected	Women eligible for routine and higher-risk breast screening
Target audience	Physicists, radiographers, radiologists
Date archived	Current

Contents

Executive summary

The purpose of the evaluation was to determine whether the Philips MicroDose SI breast imaging system meets the main standards in the NHS Breast Screening Programme (NHSBSP) and European protocols, and to provide performance data for comparison against other systems. The spectral imaging capability of this model was not tested.

The system exceeded the minimum standards in the NHSBSP and European protocols and showed an improvement in image quality compared to previous measurements on the MicroDose L30 model. The SI has two collimators, allowing larger breasts to be imaged. The use of the high collimator for larger breasts produced images of similar quality to those produced using the low collimator. As with the L30, higher doses cannot be given to larger breasts. This limits image quality to close to the minimum standard rather than the achievable level for large breasts.

1. Introduction

1.1 Testing procedures and performance standards for digital mammography

This report is one of a series evaluating commercially available direct digital mammography (DR) systems on behalf of the NHSBSP. The testing methods and standards applied are mainly derived from NHSBSP Equipment Report 0604,[1] which is referred to in this document as “the NHSBSP protocol”. The standards for image quality and dose are the same as those provided in the European protocol,[2,3] but the latter has been followed where it provides a more detailed performance standard: for example, for the automatic exposure control (AEC) system.

1.2 Objectives

The purpose of these tests was to measure the performance of the MicroDose SI breast imaging system and compare it with that of the previous model, the MicroDose L30.[4, 5]

The objectives included measuring dose and image quality for both collimators described in Section 2.1.

2. Methods

2.1 System tested

The tests were conducted at the Breast Unit at Addenbrooke's Hospital, Cambridge, on a Philips MicroDose SI system as described in Table 1.

The SI has a new detector system, the L50. It differs from the L30 in that it is designed to permit spectral imaging. However, this optional upgrade, which is not generally available, was not evaluated.

The SI has two types of collimator, referred to as "high" and "low". The low collimator is similar to that used in the L30. The high collimator allows the system to image breasts that are larger than was possible with the L30. It should only be used for breasts more than 100mm thick, so the low collimator is in use for most exposures.

Table 1. System description

Manufacturer	Philips
Model	MicroDose SI
System serial number	800369-10
Target material	Tungsten
Added filtration	500µm aluminium
Detector type	L50 photon counting silicon detector
Detector serial number	115654-10
Pixel size	50µm (at table surface)
Detector area	245.74mm x 267.75mm
Pixel array	4915 x 5355
Pixel value offset	0
Source to detector distance	660mm
Source to table distance	640.5mm
AEC modes	Smart AEC, Automatic
Software version	9.0 P1\2.1 (457)\4.0 (5916)\CCS Version 4.0 (5876)

Two AEC modes, "Automatic" and "Smart AEC", are available for use on the SI. The system defaults to the Smart AEC mode for every exposure and needs to be changed to Automatic when this mode is required.

Smart AEC selects the tube voltage and a target signal-to-noise ratio (SNR) based on the measured compression thickness. The scan velocity is then adjusted during the exposure, based on the measured detector signal, in order to give the appropriate exposure for any breast density. This mode is similar to that available on the earlier L30 model, which varies the scan velocity according to the attenuation of the breast being imaged.

The Automatic mode has no feedback during the scan. The scan velocity is constant and is based on the expected breast density and transmission for the compressed breast thickness.

Only one dose level, comparable to the higher dose level (C120) on the L30, was available on the system tested.

2.2 Output and half-value-layer

The output and half-value-layer (HVL) were measured as described in the NHSBSP protocol, at intervals of 3kV.

2.3 Detector response

The detector response was measured as described in the NHSBSP protocol, but with a different attenuator. The attenuator used was 2mm aluminium placed on the raised paddle. This is a suitable alternative to the 45mm polymethyl methacrylate (PMMA) at the tube head, which is normally used in measurements that follow the protocol.

An ion chamber was positioned above the table, 40mm from the chest wall edge, to determine the incident air kerma at the detector surface for a range of manually set mAs values at 32kV. The readings were corrected to the surface of the detector using the inverse square law. No correction was made for attenuation by the table and detector cover. The images acquired at these mAs values were saved as unprocessed files and transferred to another computer for analysis. A 10mm square region of interest (ROI) was positioned on the midline, 40mm from the chest wall edge of each image. The average pixel value and the standard deviation of pixel values within that region were measured. The relationship between average pixel values and the detector entrance surface air kerma was determined.

2.4 Dose measurement

Doses were measured using the AEC in both Automatic and Smart AEC modes to expose different thicknesses of PMMA. The PMMA blocks had an area of 180mm x 240mm. The paddle height was adjusted to be equal to the equivalent breast thickness. For convenience, the aluminium square required for the contrast-to-noise ratio (CNR) measurements was included with the PMMA, as described in Section 2.5. It is thought that the measured dose is unaffected by the presence of the aluminium in Automatic mode but it may increase in Smart AEC mode.

The AEC settings such as Phantom, PMMA20, PMMA30, which are provided within the system, were used for appropriate exposures corresponding to those for breasts of the equivalent thickness. These settings give a dose equal to the dose to breasts of the corresponding equivalent thickness, as shown in Table 2. Smart AEC ensures that the mAs is selected on the basis of transmission.

Mean glandular doses (MGDs) were calculated for all the exposures.

2.5 Contrast-to-noise ratio

To measure the CNR, an aluminium square, 10mm x 10mm and 0.2mm thick, was placed between two 10mm thick blocks of PMMA, with one edge on the midline, 60mm from the chest wall edge. Additional layers of PMMA were placed on top of these to vary the total thickness. Both Smart AEC and Automatic modes were used to make measurements for each thickness.

The images were analysed to obtain the CNRs. Twenty small square ROIs (approximately 2.5mm x 2.5mm) were used to determine the average signal and the standard deviation in the signal within the image of the aluminium square (4 ROI) and the surrounding background (16 ROI), as shown in Figure 1. Small ROIs are used to minimise distortions due to the heel effect and other causes of non-uniformity.[6] This is less important for DR systems than in computed radiography systems because a flat-field correction is applied. The CNR was calculated for each image.

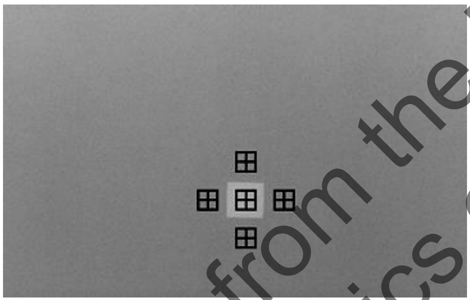

Figure 1. Location and size of ROI used to determine the CNR

To apply the standards in the European protocol, the limiting value for CNR (using 50mm PMMA) was determined according to Equation 1. This equation determines the CNR value ($\text{CNR}_{\text{limiting value}}$) that is necessary to achieve the minimum threshold gold thickness for the 0.1mm detail (that is, $\text{threshold gold}_{\text{limiting value}}$ = 1.68µm, which is equivalent to $\text{threshold contrast}_{\text{limiting value}}$ = 23.0% using 28kV Mo / Mo). Threshold contrasts were calculated as described in the European protocol and used in Equation 1.

$$\text{CNR}_{\text{target}} = \frac{\text{CNR}_{\text{measured}} \times \text{TC}_{\text{measured}}}{\text{TC}_{\text{target}}} \qquad (1)$$

The relative CNR was then calculated according to Equation 2 and compared with the limiting values provided for relative CNR shown in Table 2. The minimum CNR required to meet this criterion was then calculated.

$$\text{Relative CNR} = \text{CNR}_{\text{measured}} / \text{CNR}_{\text{limiting value}} \quad (2)$$

Table 2. Limiting values for relative CNR

Thickness of PMMA (mm)	Equivalent breast thickness (mm)	Limiting values for relative CNR (%) in European protocol
20	21	>115
30	32	>110
40	45	>105
45	53	>103
50	60	>100
60	75	>95
70	90	>90

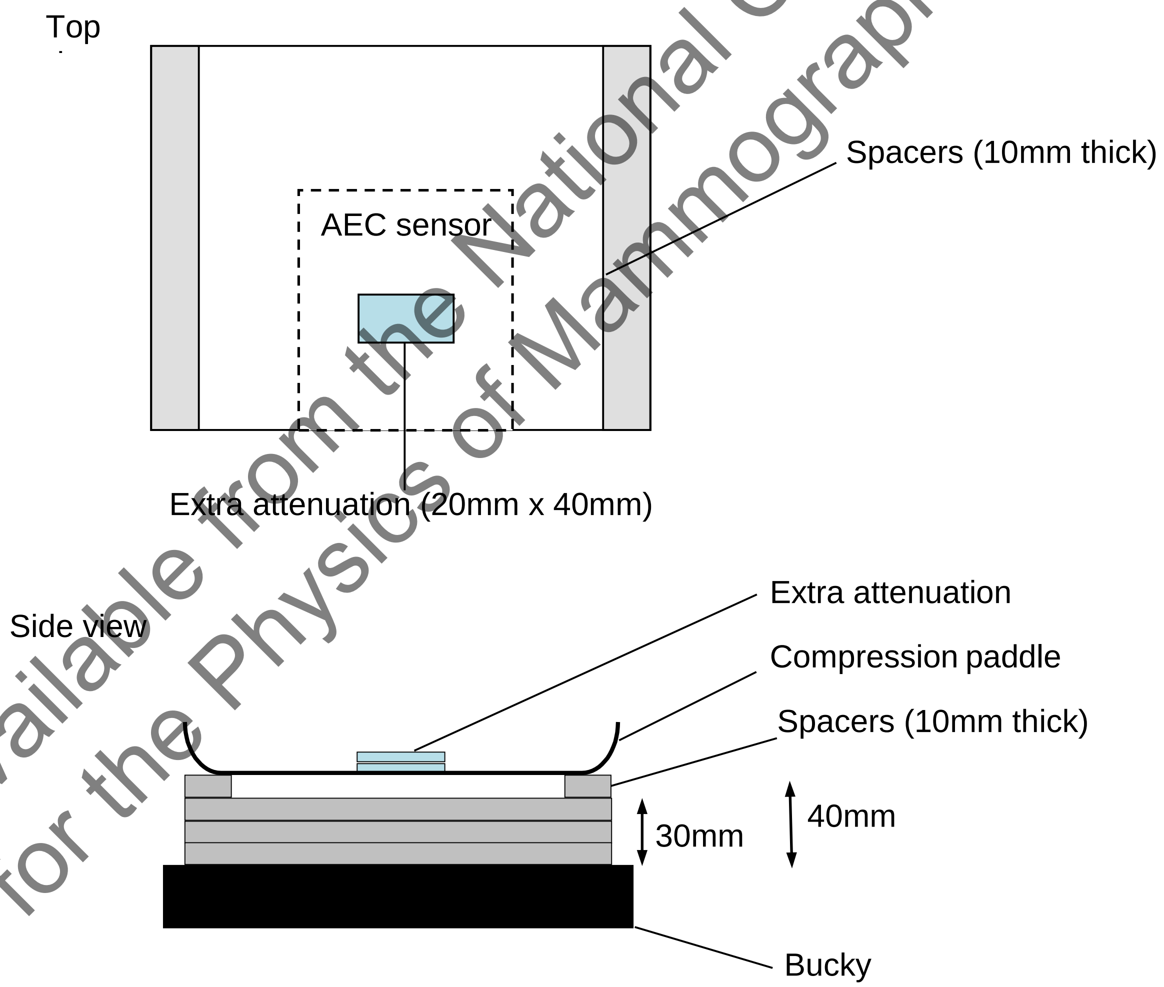

Figure 2. Setup to measure AEC performance for local dense areas

2.6 AEC performance for local dense areas

The method used in the European protocol[3] was followed. To simulate local dense areas, eleven images were made with different thicknesses (2–20mm) of extra attenuation added, so that the compression plate remained in position at 40mm height, as shown in Figure 2.

In the area of the extra attenuation (20mm x 40mm PMMA) the mean pixel value and standard deviation of 2.5mm x 2.5mm ROI were measured and the SNR calculated.

2.7 Noise analysis

The images acquired in the measurements of detector response using 32kV W / Al were used to analyse the image noise. Small ROI with an area of approximately 2.5mm x 2.5mm were placed on the midline, 60mm from the chest wall edge. The average standard deviations of the pixel values in these ROI for each image were used to investigate the relationship between the dose to the detector and the image noise. It was assumed that this noise comprises three components: electronic noise, structural noise, and quantum noise, with the relationship shown in Equation 3.

$$\sigma_p = \sqrt{k_e^2 + k_q^2 p + k_s^2 p^2} \qquad (3)$$

where σ_p is the standard deviation in pixel values within an ROI with a uniform exposure and a mean pixel value p, and k_e, k_q, and k_s are the coefficients determining the amount of electronic, quantum, and structural noise in a pixel with a value p. This method of analysis has been described previously.[7] For simplicity, the noise is generally presented here as relative noise defined as in Equation 4.

$$\text{Relative noise} = \frac{\sigma_p}{p} \qquad (4)$$

The variation in relative noise with mean pixel value was evaluated and fitted using Equation 3, and non-linear regression used to determine the best fit for the constants and their asymptotic confidence limits (using Graphpad Prism Version 4.03 for Windows, Graphpad software, San Diego, California, USA, www.graphpad.com.). This established whether the experimental measurements of the noise fitted this equation, and the relative proportions of the different noise components. In fact, the relationship between noise and pixel values has been found empirically to be approximated by a simple power relationship as shown in Equation 5.

$$\frac{\sigma_p}{p} = k_t p^{-n} \qquad (5)$$

where k_t is a constant. If the noise were purely quantum noise, the value of n would be 0.5. However, the presence of electronic and structural noise means that n can be slightly higher or lower than 0.5.

The variance in pixel values within a ROI is defined as the standard deviation squared. The total variance was plotted against incident air kerma at the detector and fitted using Equation 3. Non-linear regression was used to determine the best fit for the constants and their asymptotic confidence limits, using the Graphpad Prism software.

Using the calculated constants the structural, electronic, and quantum components of the variance were estimated, assuming that each component was independently related to incident air kerma. The percentage of the total variance represented by each component was then calculated and plotted against incident air kerma at the detector. From this, the dose range over which the quantum component dominates can be estimated.

2.8 Image quality measurements

Contrast detail measurements were made using a CDMAM phantom (serial number 1022, version 3.4, UMC St. Radboud, Nijmegen University, Netherlands). The phantom was positioned with a 20mm thickness of PMMA above and below, to give a total attenuation approximately equivalent to 50mm of PMMA or 60mm thickness of typical breast tissue. The kV and mAs were chosen to match as closely as possible that selected by the AEC when imaging a 50mm thickness of PMMA. This procedure was repeated to acquire a representative sample of 16 images at this dose level, for both low and high collimators. Further images of the test phantom were then acquired at half and double this dose level, using the low collimator. Unprocessed images were transferred to disk for subsequent analysis off-site.

An automatic method of reading the CDMAM images was used.[7, 8] Version 1.6 of CDCOM was used in the analysis. This detects the special geometry of Philips MicroDose images of the test object and correctly determines the appropriate detail positions when reading the images. The threshold gold thickness for a typical human observer was predicted using Equation 6.

$$TC_{predicted} = rTC_{auto} \quad (6)$$

where $TC_{predicted}$ is the predicted threshold contrast for a typical observer and TC_{auto} is the threshold contrast measured using an automated procedure with CDMAM images. Contrasts were calculated from gold thickness for a nominal tube voltage of 28kV with a Mo / Mo target/filter combination, as described in the European protocol; r is the average ratio between human and automatic threshold contrast determined experimentally with the values shown in Table 3.[8]

Table 3. Values of r used to predict threshold contrast

Diameter of gold disc (mm)	Average ratio of human to automatically measured threshold contrast (r)
0.08	1.40
0.10	1.50
0.13	1.60
0.16	1.68
0.20	1.75
0.25	1.82
0.31	1.88
0.40	1.94
0.50	1.98
0.63	2.01
0.80	2.06
1.00	2.11

The main advantage of automatic reading is that it has the potential for eliminating observer error, which is a significant problem when using human observers. However, it should be noted that at the time of the evaluation, the official protocols were based on human reading.

The predicted threshold gold thicknesses were fitted with curves, as described in the NHSBSP protocol. Confidence limits for the predicted threshold gold thicknesses were previously determined by a re-sampling method using a large set of images. The threshold contrasts quoted in the tables of results were derived from the fitted curves, as this has been found to improve accuracy.[8]

The expected relationship between threshold contrast and dose is shown in Equation 7.

$$\text{Threshold contrast} = \lambda D^{-n} \qquad (7)$$

where D represents the MGD for a 60mm thick standard breast equivalent to the test phantom configuration used for the image quality measurement and λ is a constant to be fitted. It is assumed that a similar equation applies when using threshold gold thickness instead of contrast. This equation was plotted with the experimental data for each detail size from 0.1 to 1.0mm. The value of n resulting in the best fit to the experimental data was determined.

3. Results

3.1 Output and HVL

The output and HVL measurements are shown in Table 4.

Table 4. Output and HVL

kV	Target / filter	Output (µGy/mAs at 1 m)	HVL (mm Al)
26	W / Al	35.2	0.35
29	W / Al	47.2	0.39
32	W / Al	60.0	0.44
35	W / Al	73.2	0.48
38	W / Al	86.9	0.52

3.2 Detector response

The detector response measured at 32kV is shown in Figure 3.

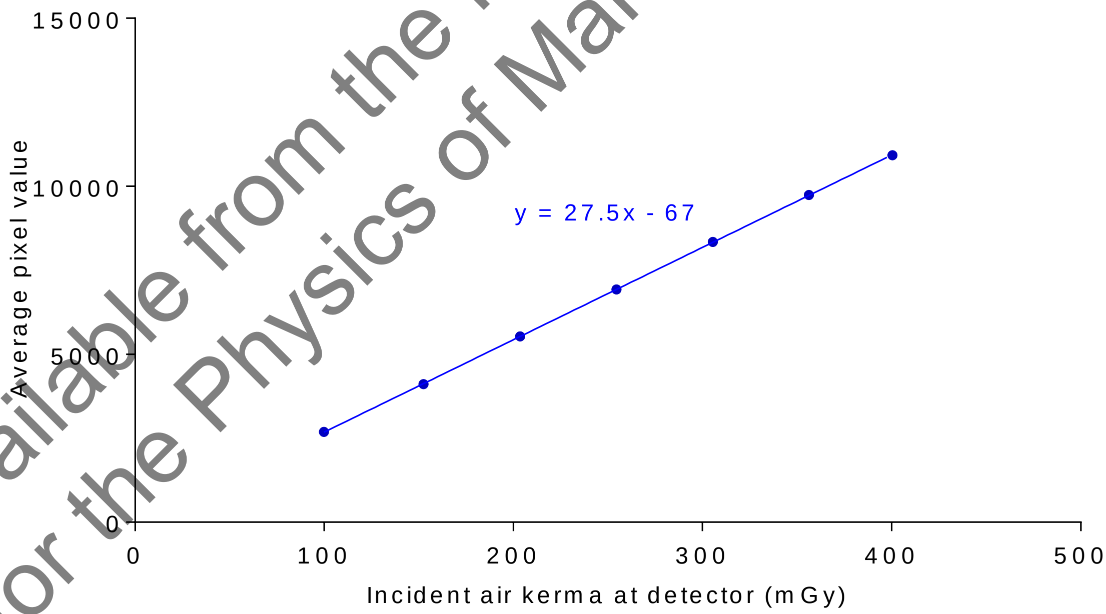

Figure 3. Detector response

3.3 AEC performance

3.3.1 Dose

The MGDs for breasts simulated with PMMA exposed under AEC control are shown in Table 5 and Figure 4. At all thicknesses, the dose was below the remedial level in the NHSBSP protocol, which is the same as the maximum acceptable level in the European protocol. The Smart AEC increased the dose by about 13% as compared to the Automatic mode due to the presence of the aluminium contrast object. The high collimator increased doses by about 9% at all thicknesses, as compared to the low collimator (both in Smart AEC mode).

Table 5. MGD for simulated breasts

PMMA thickness (mm)	Equivalent breast thickness (mm)	kV	Target / filter	Low collimator Automatic AEC		Low collimator Smart AEC		High collimator Smart AEC	
				mAs	MGD (mGy)	mAs	MGD (mGy)	mAs	MGD (mGy)
20	21	29	W / Al	7.8	0.42	8.8	0.47	9.6	0.51
30	32	32	W / Al	9.1	0.54	10.3	0.61	11.2	0.66
40	45	32	W / Al	10.6	0.53	11.8	0.58	12.9	0.64
45	53	32	W / Al	12.6	0.57	14.3	0.65	15.6	0.70
50	60	35	W / Al	13.3	0.76	14.9	0.85	16.2	0.92
60	75	38	W / Al	16.1	1.08	18.2	1.22	19.9	1.33
70	90	38	W / Al	15.8	0.93	17.9	1.05	19.6	1.15
80	107	38	W / Al	15.0	0.77	17.2	0.88	18.7	0.96
85	116	38	W / Al	14.7	0.73	16.6	0.82	18.1	0.89

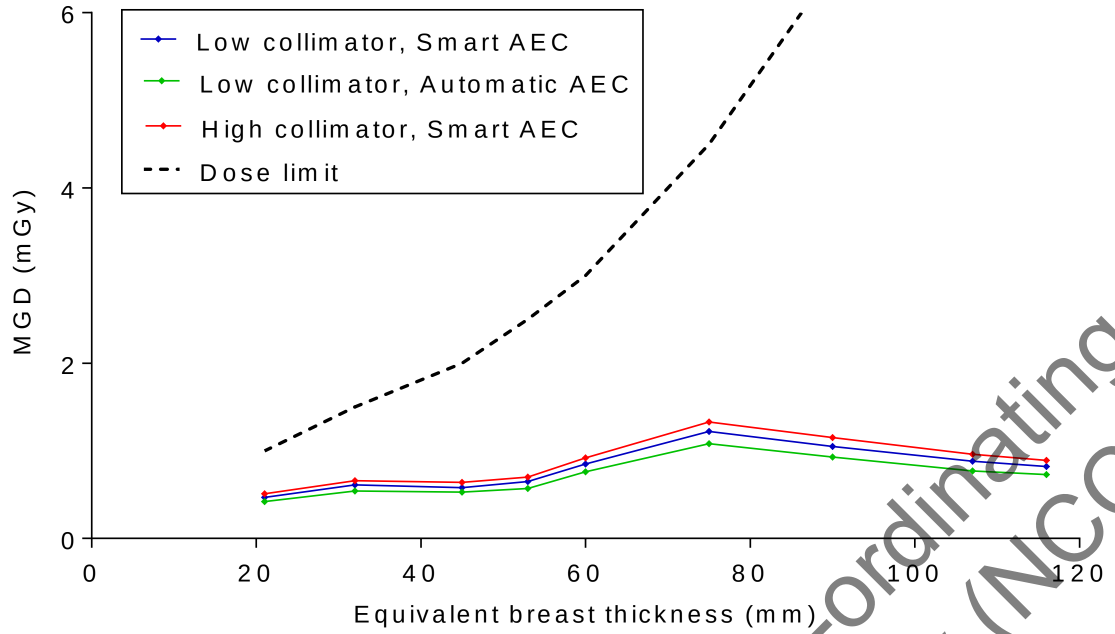

Figure 4. MGD for different thicknesses of simulated breasts using both collimators and Smart and Automatic AEC modes

3.3.2 CNR

The results of the CNR measurements are shown in Tables 6a and 6b and Figures 5a and 5b. The CNRs required to meet the minimum acceptable and achievable image quality standards at the 60mm breast thickness were calculated and are shown in Tables 6a and 6b and Figures 5a and 5b. The CNRs required at each thickness to meet the limiting CNR values in the European protocol are also shown.

Table 6a. CNR measurements using low collimator

PMMA thickness (mm)	Equivalent breast thickness (mm)	Measured CNR (Smart AEC)	Measured CNR (Automatic AEC)	CNR for minimum IQ	CNR for achievable IQ	European limiting CNR value
20	21	10.5	9.7	4.4	6.6	5.0
30	32	8.6	8.0	4.4	6.6	4.8
40	45	6.7	6.2	4.4	6.6	4.6
45	53	6.2	5.8	4.4	6.6	4.5
50	60	6.1	5.7	4.4	6.6	4.4
60	75	5.7	5.3	4.4	6.6	4.1
70	90	4.9	4.5	4.4	6.6	3.9
80	107	4.4	4.1	4.4	6.6	
85	116	4.2	4.0	4.4	6.6	

Table 6b. CNR measurements using high collimator

PMMA thickness (mm)	Equivalent breast thickness (mm)	Measured CNR (Smart AEC)	CNR for minimum IQ	CNR for achievable IQ	European limiting CNR value
20	21	11.1	3.9	5.9	4.4
30	32	9.2	3.9	5.9	4.2
40	45	7.0	3.9	5.9	4.0
45	53	6.5	3.9	5.9	4.0
50	60	6.4	3.9	5.9	3.9
60	75	5.9	3.9	5.9	3.7
70	90	5.1	3.9	5.9	3.5
80	107	4.7	3.9	5.9	
85	116	4.5	3.9	5.9	

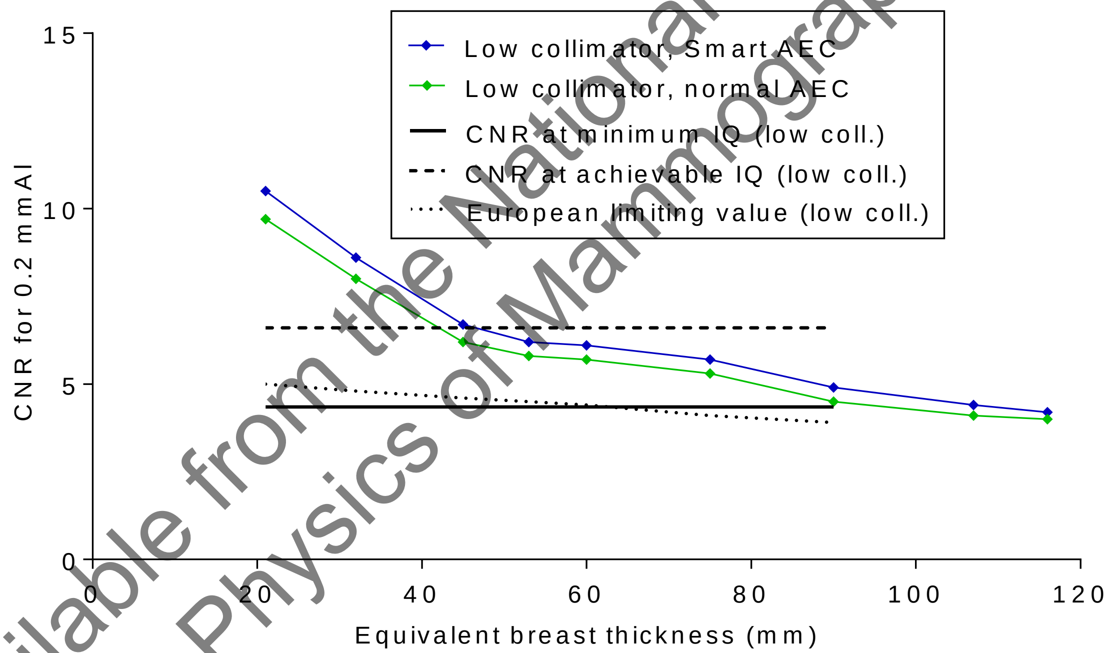

Figure 5a. Measured CNR compared with the limiting values in the European protocol for low collimator and two AEC modes. (Error bars indicate 95% confidence limits.)

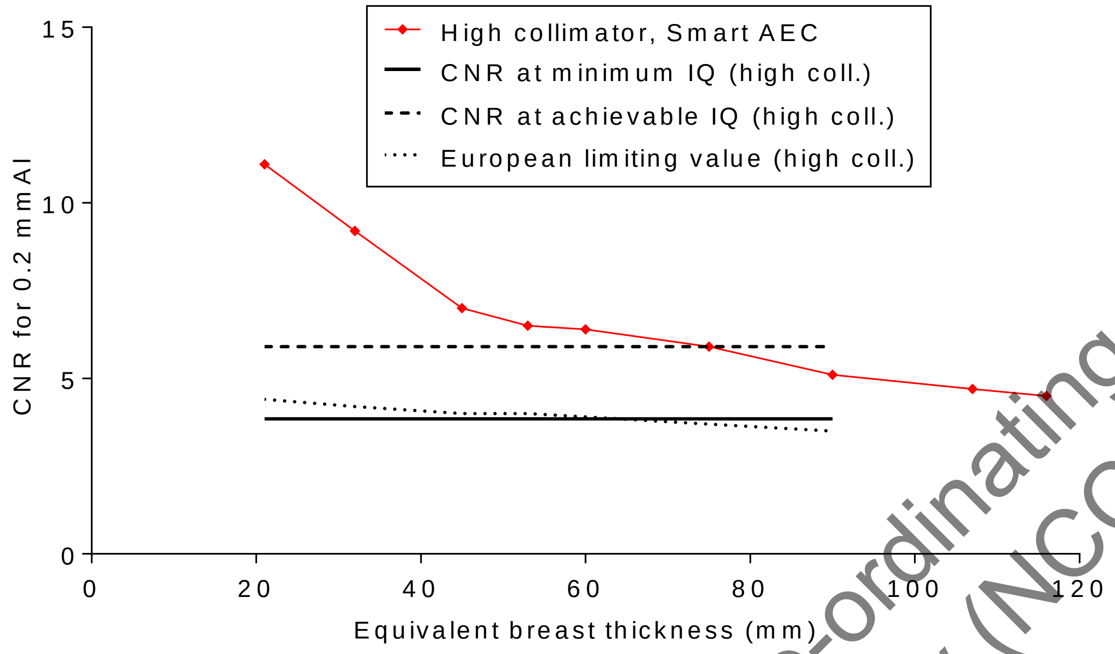

Figure 5b. Measured CNR compared with the limiting values in the European protocol for the high collimator and Smart AEC mode. (Error bars indicate 95% confidence limits.)

3.3.3 AEC performance for local dense areas

The SNR is expected to remain constant with increasing thickness of extra PMMA when the AEC adjusts for locally dense areas. The results presented in Table 7 and Figure 6 show that the SNR remains nearly constant as thickness increases.

Table 7. AEC performance for local dense areas

Attenuation (mm PMMA)	Target / filter	Tube voltage (kV)	Tube load (mAs)	SNR	% difference from mean SNR
30	W / Al	32	6.7	56.5	2
32	W / Al	32	7.2	56.2	1
34	W / Al	32	7.8	56.1	1
36	W / Al	32	8.4	55.8	0
38	W / Al	32	9.0	55.8	0
40	W / Al	32	9.7	55.8	0
42	W / Al	32	10.5	55.6	0
44	W / Al	32	11.3	55.2	-1
46	W / Al	32	12.3	55.1	-1
48	W / Al	32	13.1	54.6	-2
50	W / Al	32	14.2	54.6	-2

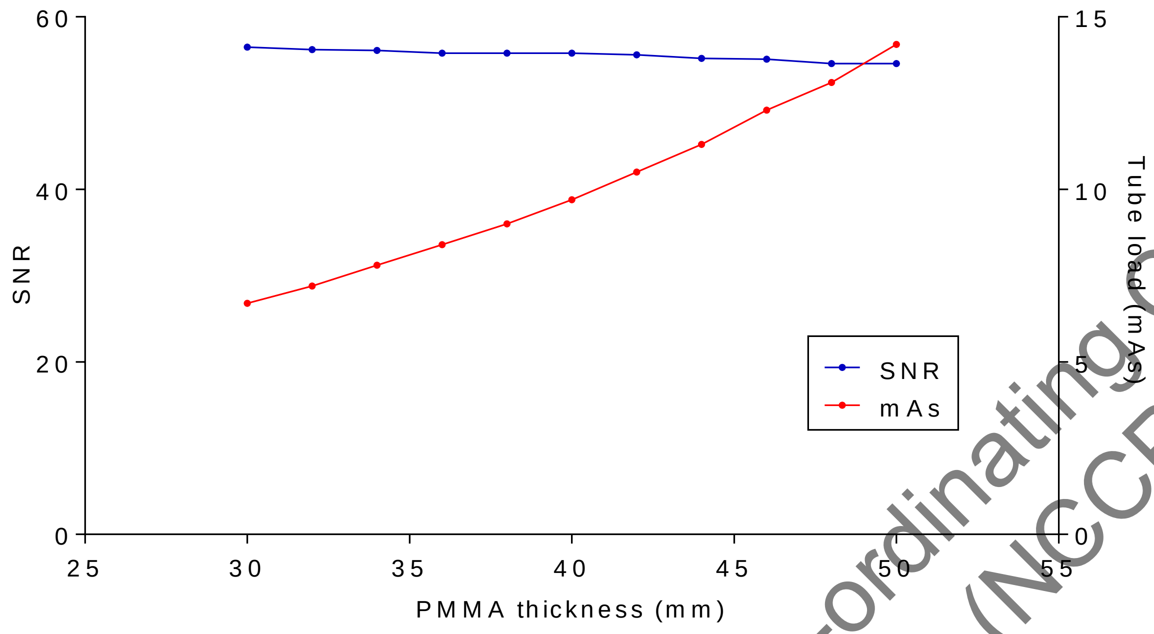

Figure 6. AEC performance for local dense areas

3.4 Noise measurements

The variation in noise with dose was analysed by plotting the standard deviation in pixel values against the detector entrance air kerma, as shown in Figure 7. The fitted power curve has an index of 0.51, close to the value of 0.50 which would be expected if quantum noise sources alone were present.

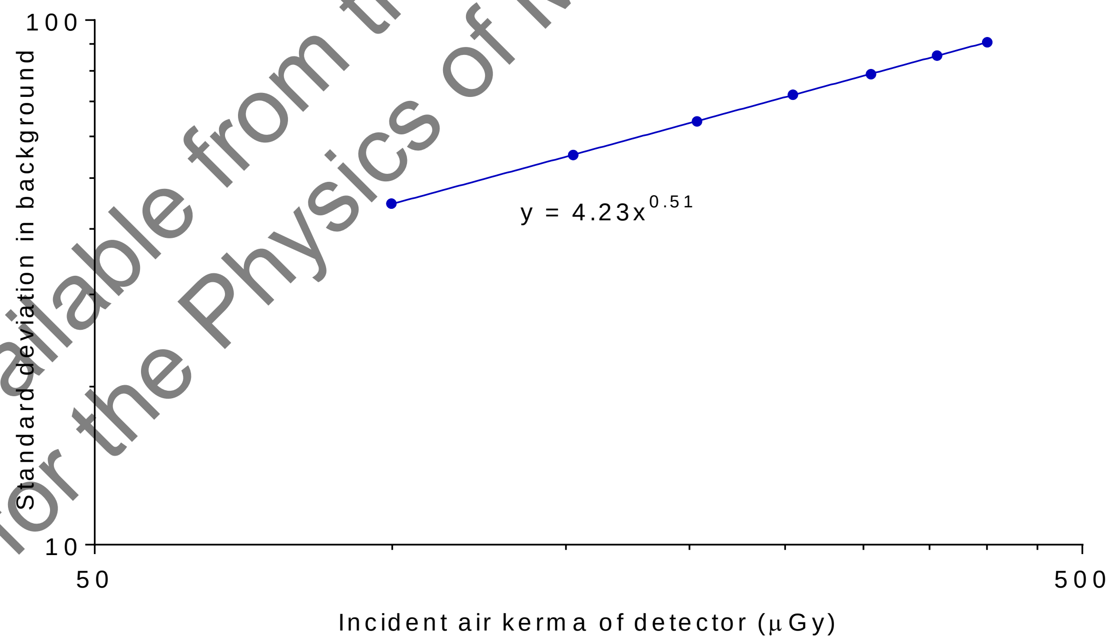

Figure 7. Standard deviation of pixel values versus air kerma at detector

Figure 8 is an alternative way of presenting the data and shows the relative noise at different entrance air kerma. The estimated relative contributions of electronic, structural, and quantum noise are shown and the quadratic sum of these contributions fitted to the measured noise (using Equation 3).

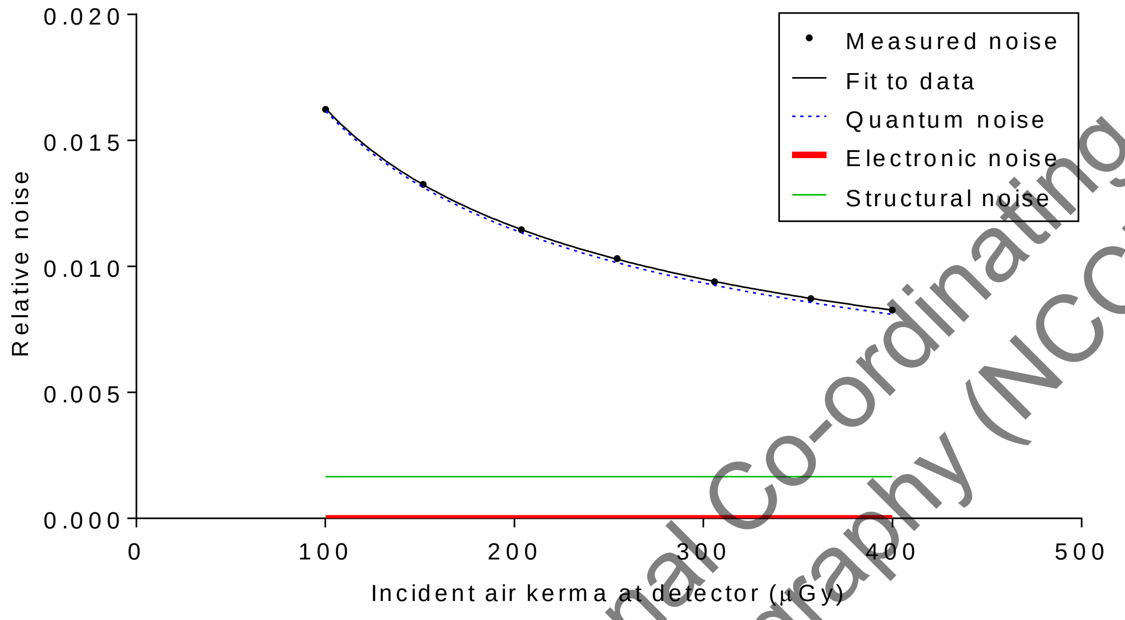

Figure 8. Relative noise and noise components

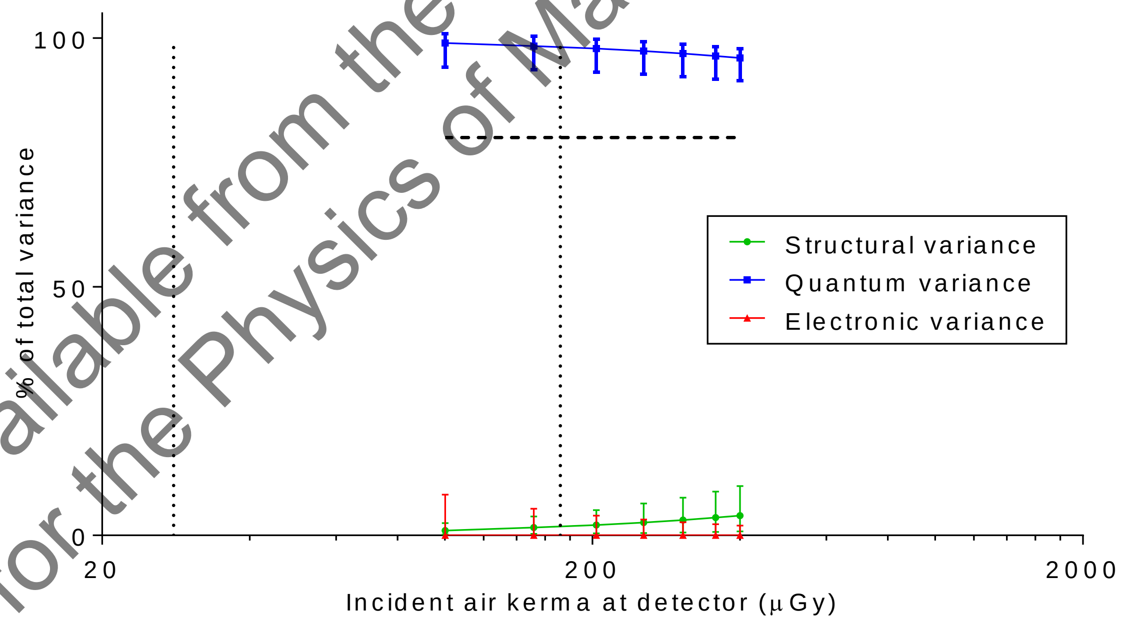

Figure 9. Noise components as a percentage of the total variance. (Error bars indicate 95% confidence limits.)

Figure 9 shows the different amounts of variance due to each component. Quantum noise predominates and electronic noise is zero. The percentage quantum variance is compared to a limit of 80%. The errors were estimated assuming that the errors in each of the components were independent. The vertical dotted lines indicate the minimum and maximum incident air kerma noted during the AEC tests of different thicknesses of PMMA.

3.5 Image quality measurements

Exposures of the CDMAM using the AEC in Smart AEC mode resulted in the selection of 35kV W / Al with 13.3mAs for the low collimator and 14.8mAs for the high collimator. Details of the AEC mode and exposure factors selected are given in Table 8 with the corresponding MGDs to equivalent breasts (60mm thick).

Table 8. Images acquired for image quality measurement

Collimator	Corresponding AEC mode	kV	Target / filter	Tube loading (mAs)	MGD to equivalent breasts 60mm thick (mGy)	Number of CDMAM images acquired and analysed
low	manual	35	W / Al	6.5	0.37	16
low	Smart AEC	35	W / Al	13.3	0.76	16
low	manual	35	W / Al	23.6	1.34	16
high	Smart AEC	35	W / Al	14.8	0.84	16

The contrast detail curves at the different dose levels and different collimators (determined by automatic reading of the images) are shown in Figures 10a and 10b. The threshold gold thicknesses for selected diameters and the different dose levels and collimators are shown in Tables 9a and 9b, along with the minimum and achievable threshold values from the NHSBSP protocol (which are the same as those of the European protocol). The data in Tables 9a and 9b are taken from the fitted curves rather than raw data.

Table 9a. Average threshold gold thicknesses for different detail diameters for three doses using 35kV W / Al (low collimator) and automatically predicted data

Diameter (mm)	Threshold gold thickness (µm)				
	Acceptable value	Achievable value	MGD = 0.37mGy	MGD = 0.76mGy	MGD = 1.34mGy
0.1	1.680	1.100	2.135 ± 0.168	1.259 ± 0.092	0.998 ± 0.071
0.25	0.352	0.244	0.337 ± 0.027	0.228 ± 0.017	0.196 ± 0.014
0.5	0.150	0.103	0.137 ± 0.012	0.102 ± 0.008	0.070 ± 0.006
1	0.091	0.056	0.079 ± 0.010	0.050 ± 0.006	0.047 ± 0.005

The 0.76mGy column in Table 9a is that selected by the Smart AEC.

Table 9b. Average threshold gold thicknesses for different detail diameters using 35kV W / Al (Smart AEC, high collimator) and automatically predicted data

Diameter (mm)	Threshold gold thickness (µm)		
	Acceptable value	Achievable value	MGD = 0.84mGy
0.1	1.680	1.100	1.065 ± 0.081
0.25	0.352	0.244	0.249 ± 0.018
0.5	0.150	0.103	0.097 ± 0.008
1	0.091	0.056	0.050 ± 0.006

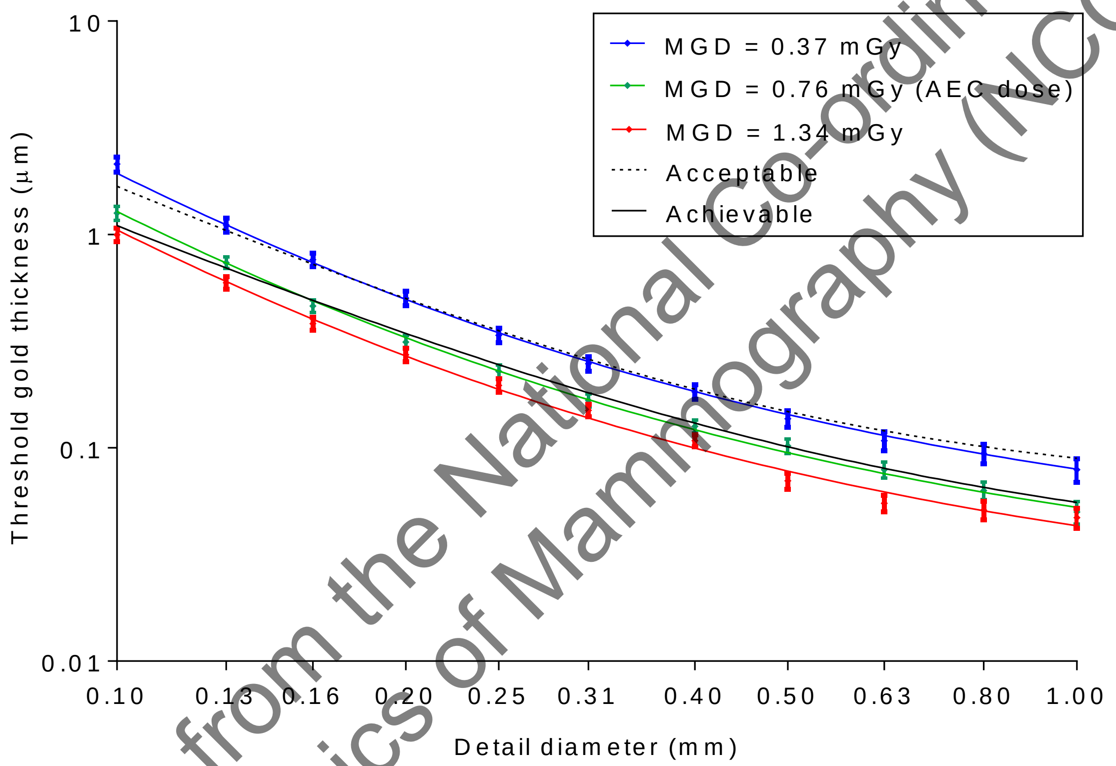

Figure 10a. Contrast-detail curves for three doses at 35kV W / Al with the low collimator. (Error bars indicate 95% confidence limits.)

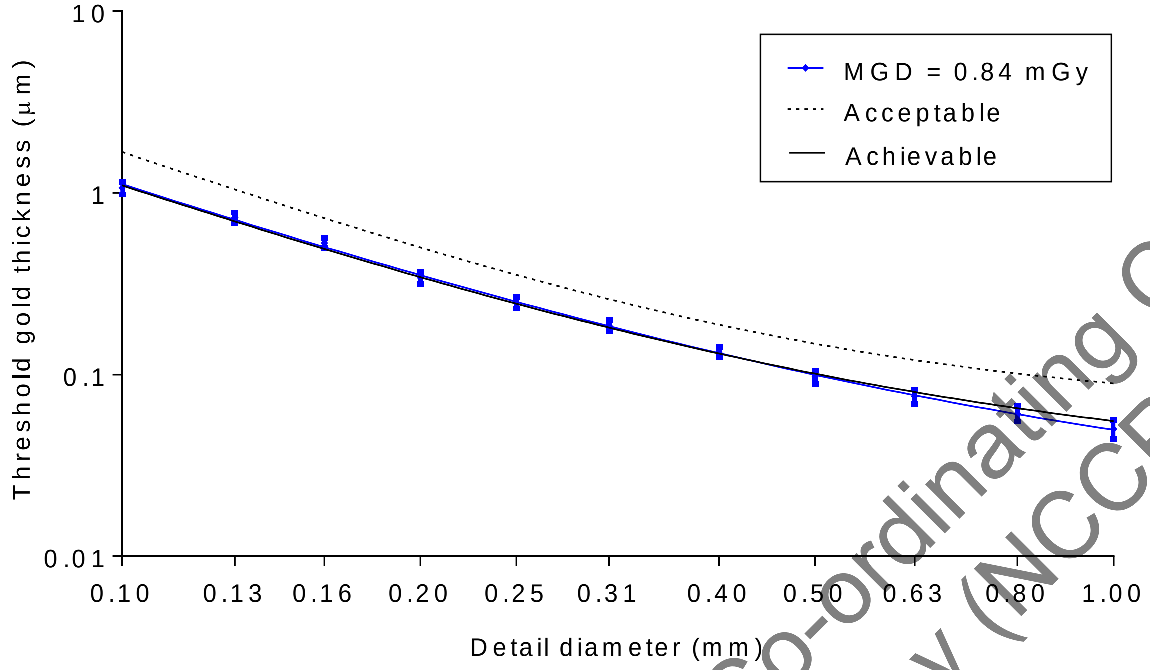

Figure 10b. Contrast-detail curves for the Smart AEC-selected dose at 35kV W / Al with the high collimator. (Error bars indicate 95% confidence limits.)

The measured threshold gold thicknesses are plotted against the MGD for an equivalent breast for the 0.1mm and 0.25mm detail sizes in Figure 11.

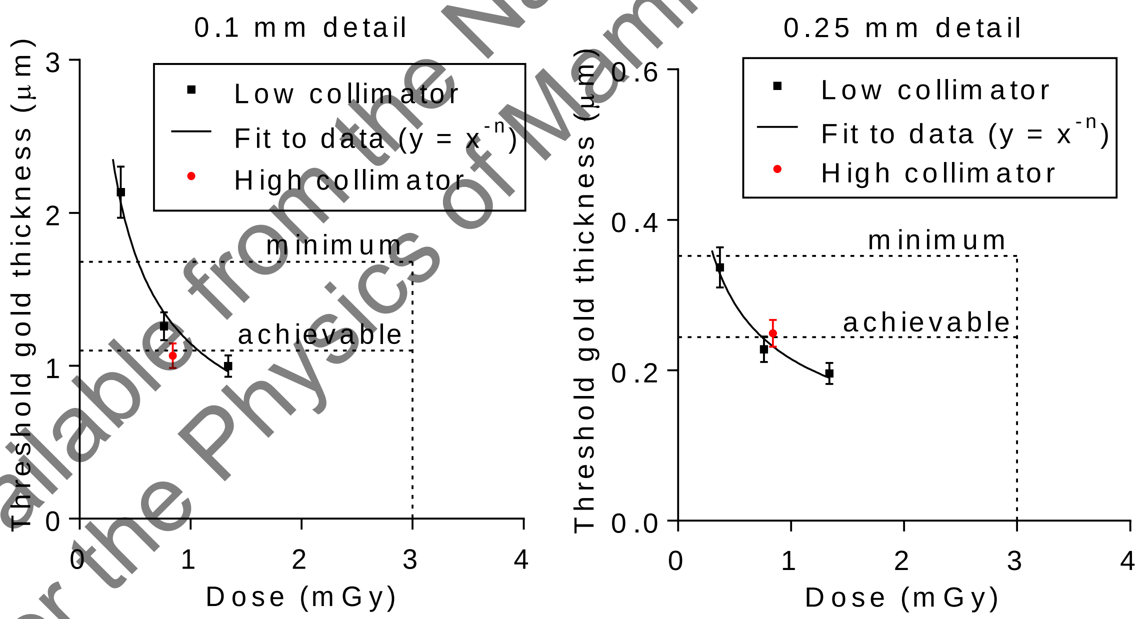

Figure 11. Threshold gold thickness at different doses. (Error bars indicate 95% confidence limits.)

3.6 Comparison with other systems

The MGDs to reach the minimum and achievable image quality standards in the NHSBSP protocol were estimated from the curves shown in Figure 11. (The error in estimating these doses depends on the accuracy of the curve fitting procedure, and pooled data for several systems has been used to estimate the 95% confidence limits of about 20%.) These doses are shown against similar data for other models of digital mammography system in Tables 10 and 11 and Figures 12 to 15. The data for the other systems was determined in the same way as described in this report and the results published previously.9-20 The data for film-screen represent an average value determined using a variety of film screen systems previously used in the NHSBSP.

Table 10. The MGD for different systems to reach the minimum threshold gold thickness for 0.1mm and 0.25mm details

System	MGD (mGy) for 0.1mm	MGD (mGy) for 0.25mm
Philips MicroDose SI (low collimator)	**0.53**	**0.32**
Philips MicroDose L30	0.67	0.47
Siemens Inspiration	0.76	0.60
Fuji Amulet f/s	0.79	0.58
Hologic Dimensions (v1.4.2)	0.34	0.48
Hologic Selenia (W)	0.71	0.64
GE Essential	0.49	0.49
IMS Giotto 3DL	0.93	0.70
Film-screen	1.30	1.36
Agfa CR (NIP)	1.27	0.96
Fuji Profect CR	1.78	1.35

Table 11. The MGD for different systems to reach the achievable threshold gold thickness for 0.1mm and 0.25mm details

System	MGD (mGy) for 0.1mm	MGD (mGy) for 0.25mm
Philips MicroDose SI (low collimator)	**1.07**	**0.74**
Philips MicroDose L30	1.34	1.06
Siemens Inspiration	1.27	1.16
Fuji Amulet f/s	1.35	1.58
Hologic Dimensions (v1.4.2)	0.87	1.10
Hologic Selenia (W)	1.37	1.48
GE Essential	1.13	1.03
IMS Giotto 3DL	1.60	1.41
Film-screen	3.03	2.83
Agfa CR (NIP)	2.47	2.34
Fuji Profect CR	3.29	2.65

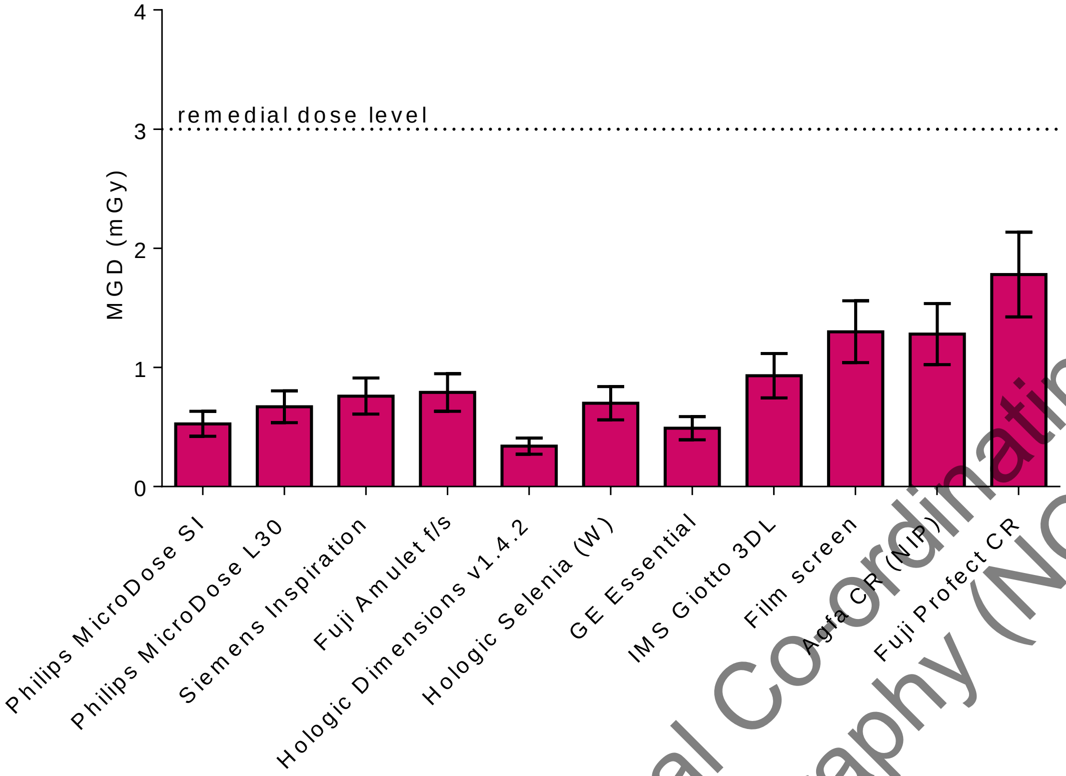

Figure 12. Dose to reach minimum acceptable image quality standard for 0.1mm details. (Error bars indicate 95% confidence limits.)

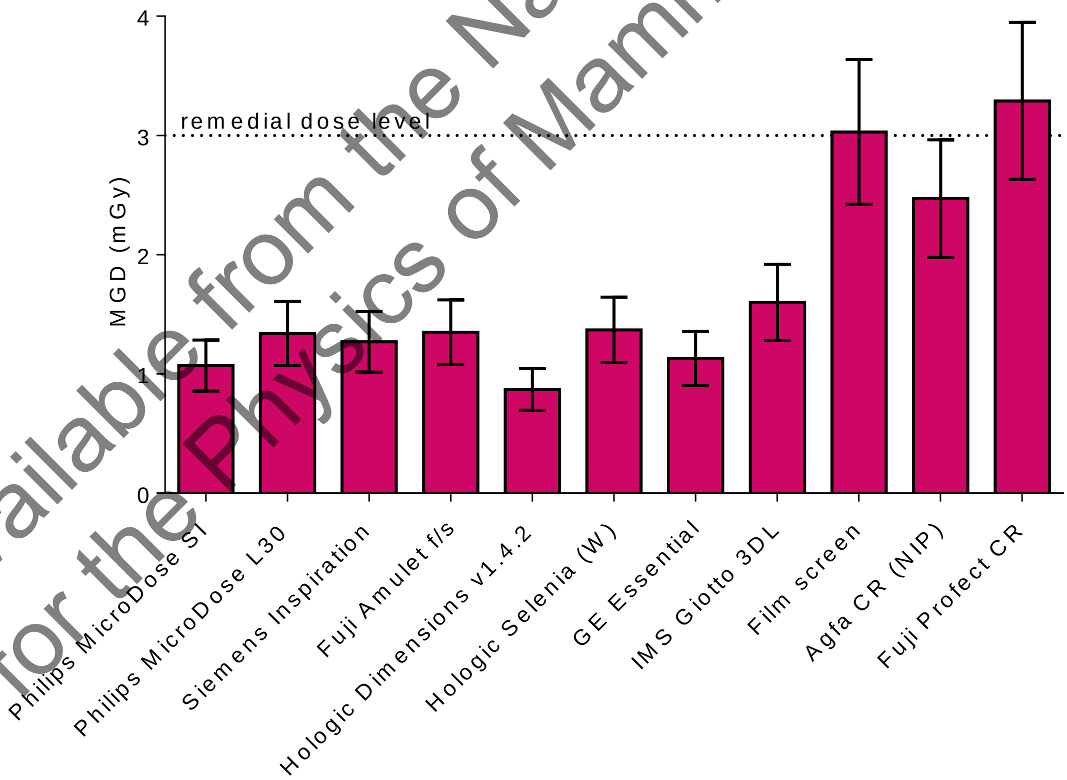

Figure 13. Dose to reach achievable image quality standard for 0.1mm details. (Error bars indicate 95% confidence limits.)

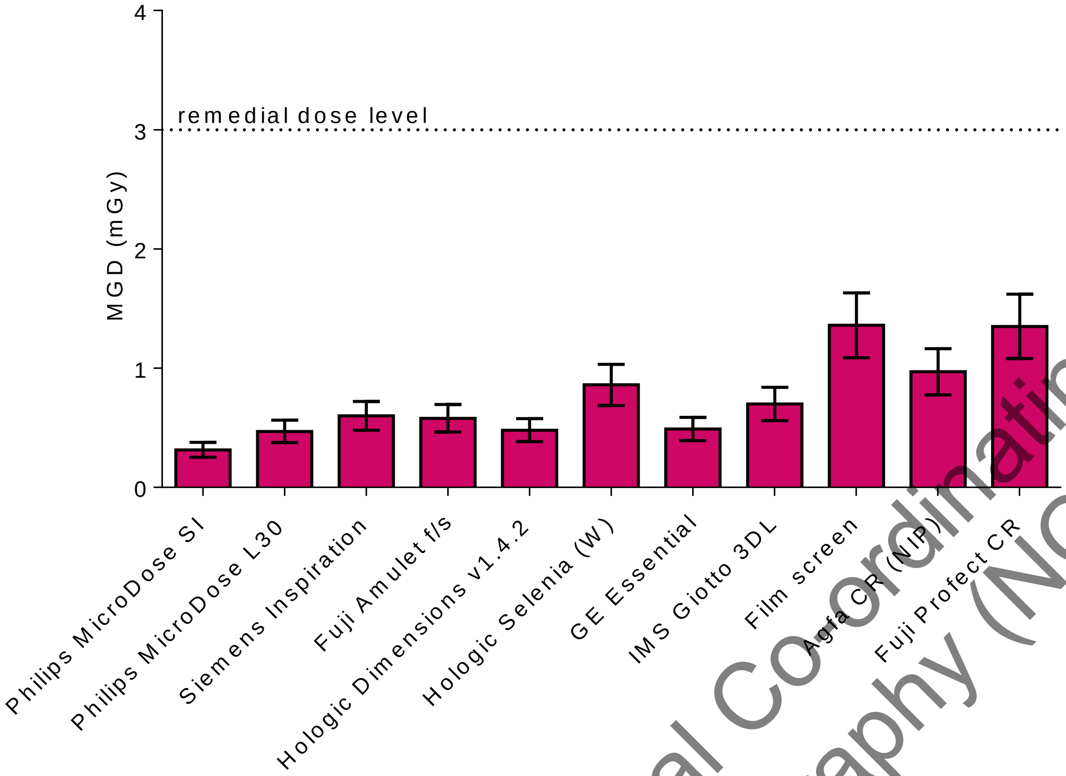

Figure 14. Dose to reach minimum acceptable image quality standard for 0.25mm details. (Error bars indicate 95% confidence limits.)

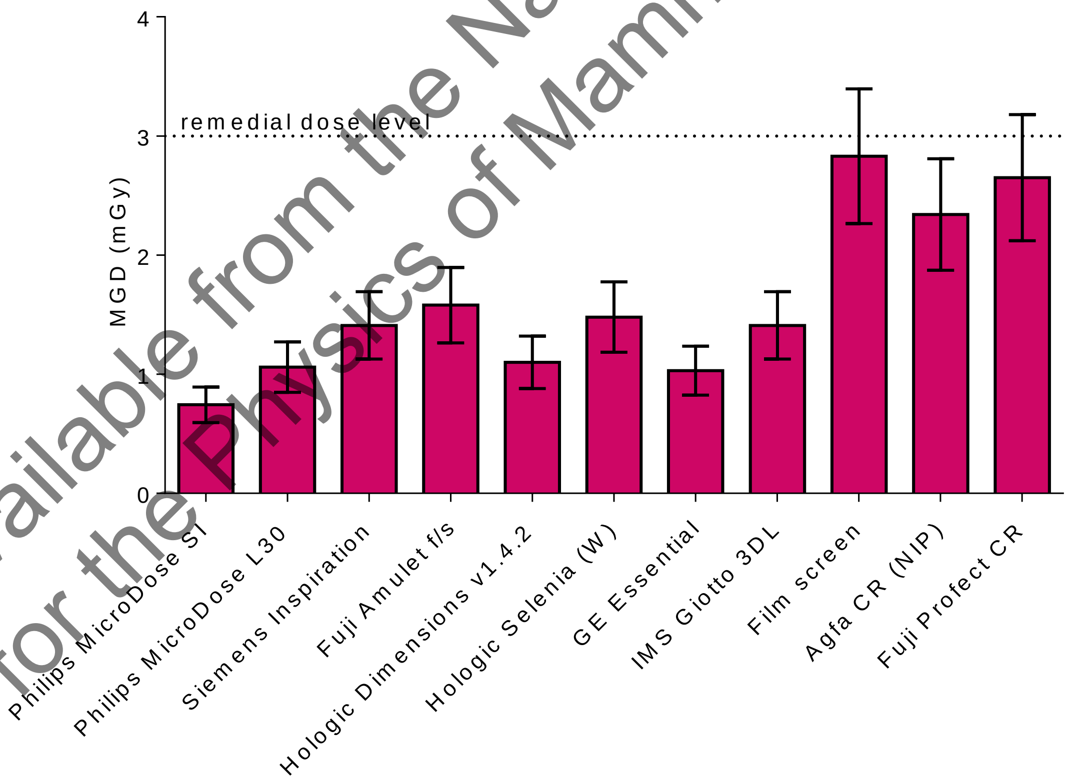

Figure 15. Dose to reach achievable image quality standard for 0.25mm details. (Error bars indicate 95% confidence limits.)

4. Discussion

The system exceeded the minimum image quality standards in all modes tested. Smart AEC was the default AEC mode on the system tested, and was set up as approximately equivalent to the higher C120 dose mode available in the L30 model.

For the low collimator, the threshold gold contrast at the AEC-selected dose was between the minimum and achievable standard for 0.1mm details but was at the achievable level for the other detail sizes. Most modern DR systems operate at or above the achievable level for all detail sizes.

The CNR values met the minimum European standard for all PMMA thicknesses but were relatively low for large breast thicknesses. The CNR was below achievable for PMMA thicknesses of 50mm and above (Figure 5a). This is a consequence of the relatively low doses for thicker breasts (Figure 4). The Smart AEC mode was effective at correcting for locally dense areas. It is recommended that this mode be used clinically.

The noise analysis found no electronic noise and only a relatively low structural noise. Thus quantum noise dominates. The lack of electronic noise is as expected, due to the photon counting nature of the system.

The doses for all modes were well below the remedial level, for example, 0.76mGy and 0.85mGy for Automatic and Smart AEC modes respectively, for the 53mm thick standard breast (45mm PMMA) as compared with the remedial level of 2.5mGy. The doses required to reach the minimum and achievable image quality standards were within the range of values which have been determined for other DR systems. In practice, the dose range available is limited. The dose was close to that required for achievable image quality at the standard thickness for image quality measurements. However, the relatively low dose used for the thicker breasts limits the quality of images for these breasts. It is surprising that the mAs selected reduces as simulated breast thicknesses increase above 75mm (Table 5), as this is the opposite of what is required to maintain image quality.

The performance using the high collimator was very similar to that using the low collimator and gave similar image quality with about 13% higher dose. Although the measurements showed a small improvement in image quality when using the high collimator as compared to the low collimator, this may be within experimental error and therefore not reproducible. The manufacturer recommends that the high collimator is used only when imaging larger breasts, of thickness greater than 100mm.

5. Conclusions

The system met all the main standards in the NHSBSP and European protocols and showed an improvement in image quality compared to previous measurements on the MicroDose L30.

As with earlier models, doses cannot be increased for the larger breasts. This limits image quality to close to the minimum rather than the achievable level for these breasts.

References

1. Workman A, Castellano I, Kulama E et al. *Commissioning and Routine Testing of Full Field Digital Mammography Systems* (NHSBSP Equipment Report 0604 Version 3). Sheffield: NHS Cancer Screening Programmes, 2009

2. Young KC, Johnson B, Bosmans H et al. The European protocol for the quality control of the physical and technical aspects of mammography screening. In: *European Guidelines for Quality Assurance in Breast Cancer Screening and Diagnosis*, 4th Edition, Luxembourg: European Commission, 2006

3. van Engen R, Bosmans H, Dance D et al. Digital mammography update: European protocol for the quality control of the physical and technical aspects of mammography screening. In: *European guidelines for quality assurance in breast cancer screening and diagnosis,* 4th edition – Supplements, Luxembourg: European Commission, 2013

4. Young KC, Oduko JM, Alsager A. *Technical Evaluation of the Sectra MDM-L30 Full Field Digital Mammography System* (NHSBSP Equipment Report 0805). Sheffield: NHS Cancer Screening Programmes, 2008

5. Oduko JM, Young KC. *Technical evaluation of the Philips MicroDose L30 with AEC software version 8.3* (NHSBSP Equipment Report 1305). Sheffield: NHS Cancer Screening Programmes, 2013

6. Alsager A, Young KC, Oduko JM. Impact of Heel Effect and ROI Size on the Determination of Contrast-to-Noise Ratio for Digital Mammography Systems. In *Proceedings of SPIE Medical Imaging*, Bellingham WA: SPIE Publications, 2008, 69134: 1-11

7. Young KC, Cook JH, Oduko JM. Automated and human determination of threshold contrast for digital mammography systems. In *Proceedings of the 8th International Workshop on Digital Mammography,* Berlin: Springer-Verlag, 2006, 4046: 266-272

8. Young KC, Alsager A, Oduko JM et al. Evaluation of software for reading images of the CDMAM test object to assess digital mammography systems. In *Proceedings of SPIE Medical Imaging*, Bellingham WA: SPIE Publications, 2008, 69131C: 1-11

9. Young KC, Oduko JM, Woolley L. *Technical Evaluation of the Hologic Selenia Full Field Digital Mammography System* (NHSBSP Equipment Report 0701). Sheffield: NHS Cancer Screening Programmes, 2007

10. Young KC, Oduko JM. *Technical Evaluation of the Hologic Selenia Full Field Digital Mammography System with a Tungsten Tube* (NHSBSP Equipment Report 0801). Sheffield: NHS Cancer Screening Programmes, 2008

11. Young KC, Oduko JM, Gundogdu O et al. *Technical Evaluation of the GE Essential Full Field Digital Mammography System* (NHSBSP Equipment Report 0803). Sheffield: NHS Cancer Screening Programmes, 2008

12. Oduko JM, Young KC, Alsager A et al. *Technical Evaluation of the IMS Giotto Full Field Digital Mammography System with a Tungsten Tube* (NHSBSP Equipment Report 0804). Sheffield: NHS Cancer Screening Programmes, 2008
13. Young KC, Oduko JM, Gundogdu O, Asad M. *Technical Evaluation of Profile Automatic Exposure Control Software on GE Essential Full Field Digital Mammography System* (NHSBSP Equipment Report 0903). Sheffield: NHS Cancer Screening Programmes, 2009
14. Young KC, Oduko JM, Asad M. *Technical Evaluation of Agfa DX-M Mammography CR Reader with HM5.0 Needle-IP* (NHSBSP Equipment Report 0905). Sheffield: NHS Cancer Screening Programmes, 2009
15. Young KC, Oduko JM, Asad M. *Technical Evaluation of Fuji Amulet Full Field Digital Mammography System* (NHSBSP Equipment Report 0907). Sheffield: NHS Cancer Screening Programmes, 2009
16. Young KC, Oduko JM, Gundogdu O, Alsager A. *Technical evaluation of Siemens Mammomat Inspiration Full Field Digital Mammography System* (NHSBSP Equipment Report 0909). Sheffield: NHS Cancer Screening Programmes, 2009
17. Young KC, Oduko JM, Warren L. *Technical evaluation of Hologic Selenia Dimensions 2-D digital breast imaging system* (NHSBSP Equipment Report 1101). Sheffield: NHS Cancer Screening Programmes, 2011
18. Young KC, Oduko JM. *Technical evaluation of Hologic Selenia Dimensions 2-D Digital Breast Imaging System with software version 1.4.2* (NHSBSP Equipment Report 1201). Sheffield: NHS Cancer Screening Programmes, 2012
19. Strudley CJ, Young KC, Oduko JM. *Technical evaluation of the IMS Giotto 3DL Digital Breast Imaging System* (NHSBSP Equipment Report 1301). Sheffield: NHS Cancer Screening Programmes, 2013
20. Oduko JM, Young KC, Warren L. *Technical evaluation of the Fuji Amulet f/s Digital Breast Imaging System* (NHSBSP Equipment Report 1304). Sheffield: NHS Cancer Screening Programmes, 2013

Appendix: Manufacturer's comments

The design of the MicroDose SI is such that the same image quality will be delivered regardless of the collimator used. The average glandular dose, however, is about 10% higher with the high collimator. The slightly better image quality for the high collimator reported here is consistent with this given the measurement uncertainties. We therefore urge the users to use the upper collimator only when necessary.

The manufacturer wants to reiterate the statement from Section 2.8: "However, it should be noted that at the present time the official protocols are based on human reading." It should also be noted that the Philips MicroDose L30 in the previous report[4] had significantly better human than predicted performance for the 0.1mm disc. In that report, the MGD to reach minimum threshold thickness for human scoring of the 0.1mm disc was 0.41mGy, which was 41% lower than the predicted value. This discrepancy is consistent with what we have seen in internal evaluations, and the published data in the 510(K)-application for regulatory clearance of Philips MicroDose L30 in the USA is consistent with the lower dose value.